


# Sensing the heavy water concentration in an $H_2O$-$D_2O$ mixture by solid-solid phononic crystals

Mohammadreza Rahimi and Ali Bahrami

**Citation:**Chin. Phys. B, 2024, 33 (**4**): 044301. DOI: 10.1088/1674-1056/ad0bf5
Journal homepage: http://cpb.iphy.ac.cn; http://iopscience.iop.org/cpb

**What follows is a list of articles you may be interested in**

---

## Nonlinear wave propagation in acoustic metamaterials with bilinear nonlinearity

Shiqi Liang(梁诗琪), Jiehui Liu(刘杰惠), Yun Lai(赖耘), and Xiaozhou Liu(刘晓宙)
Chin. Phys. B, 2023, 32 (**4**): 044301. DOI: 10.1088/1674-1056/ac9783

## Tunable topological interface states and resonance states of surface waves based on the shape memory alloy

Shao-Yong Huo(霍绍勇), Long-Chao Yao(姚龙超), Kuan-Hong Hsieh(谢冠宏), Chun-Ming Fu(符纯明), Shih-Chia Chiu(邱士嘉), Xiao-Chao Gong(龚小超), and Jian Deng(邓健)
Chin. Phys. B, 2023, 32 (**3**): 034303. DOI: 10.1088/1674-1056/ac8727

## Analysis on vibration characteristics of large-size rectangular piezoelectric composite plate based on quasi-periodic phononic crystal structure

Li-Qing Hu(胡理情), Sha Wang(王莎), and Shu-Yu Lin(林书玉)
Chin. Phys. B, 2022, 31 (**5**): 054302. DOI: 10.1088/1674-1056/ac3649

## Broadband topological valley-projected edge-states transport in composite structure phononic crystal

Hong-Yong Mao(毛鸿勇), Fu-Jia Chen(陈福家), Kai Guo(郭凯), and Zhong-Yi Guo(郭忠义)
Chin. Phys. B, 2021, 30 (**8**): 084302. DOI: 10.1088/1674-1056/abea89

## Impact vibration properties of locally resonant fluid-conveying pipes

Bing Hu(胡兵), Fu-Lei Zhu(朱付磊), Dian-Long Yu(郁殿龙), Jiang-Wei Liu(刘江伟), Zhen-Fang Zhang(张振方), Jie Zhong(钟杰), and Ji-Hong Wen(温激鸿)
Chin. Phys. B, 2020, 29 (**12**): 124301. DOI: 10.1088/1674-1056/abb312

---

# Sensing the heavy water concentration in an $H_2O$–$D_2O$ mixture by solid–solid phononic crystals

Mohammadreza Rahimi and Ali Bahrami[†]

*Optoelectronic and Nanophotonics Research Laboratory (ONRL), Faculty of Electrical Engineering, Sahand University of Technology, Tabriz, Iran*

(Received 22 July 2023; revised manuscript received 10 November 2023; accepted manuscript online 13 November 2023)

A new method based on phononic crystals is presented to detect the concentration of heavy water ($D_2O$) in an $H_2O$–$D_2O$ mixture. Results have been obtained and analyzed in the concentration range of 0%–10% and 90%–100% $D_2O$. A proposed structure of tungsten scatterers in an aluminum host is studied. In order to detect the target material, a cavity region is considered as a sound wave resonator in which the target material with different concentrations of $D_2O$ is embedded. By changing the concentration of $D_2O$ in the $H_2O$–$D_2O$ mixture, the resonance frequency undergoes a frequency shift. Each 1% change in $D_2O$ concentration in the $H_2O$–$D_2O$ mixture causes a frequency change of about 120 Hz. The finite element method is used as the numerical method to calculate and analyze the natural frequencies and transmission spectra of the proposed sensor. The performance evaluation index shows a high $Q$ factor up to 1475758 and a high sensitivity up to 13075, which are acceptable values for sensing purposes. The other figures of merit related to the detection performance also indicate high-quality performance of the designed sensor.

**Keywords:** phononic crystals, sensor, $H_2O$–$D_2O$ mixture, cavity

**PACS:** 43.20.+g, 43.40.+s, 43.58.+z **DOI:** 10.1088/1674-1056/ad0bf5

## 1. Introduction

Deuterium oxide ($D_2O$), or heavy water, has a heavier isotope of hydrogen called deuterium in its molecular structure. This causes $D_2O$ to have different physical properties from normal water.[1] Deuterium oxide is used in many scientific and industrial applications such as nuclear reactions, magnetic nuclear resonance, as a coolant in nuclear power plants[2] and for metabolic isotope labeling in biological processes.[3]

Different methods have been implemented for heavy water production. Water electrolysis, water distillation and hydrogen distillation were investigated as hydrogen–deuterium separation methods to achieve deuterium vapor and its separation from regular hydrogen.[4] Because of the similar chemical properties of $D_2O$ and $H_2O$, discrimination between them is tremendously hard. There exist some laser-based methods, luminescent material methods and nanocrystal methods to trace $D_2O$ in an $H_2O$–$D_2O$ mixture.[5,6] Due to the physical differences between $D_2O$ and $H_2O$, other sensing methods such as phononic crystals (PhCs) can be used for this purpose. PhCs can be utilized to detect the concentration of a substance in a compound or to distinguish two or more substances from each other.[7,8]

PhCs are fabricated structures made to control and manipulate acoustic waves, and include two or more materials with diverse physical properties in elasticity, mass density and speed of sound.[9,10] The inclusion materials can be embedded in the host with one-dimensional (1D),[11,12] two-dimensional (2D)[13,14] or three-dimensional (3D)[15] arrangements. The periodic property of these structures creates one or more forbidden regions in the corresponding diagram band, the phononic band gap.[16] The phononic band gap plays an important role in acoustic wave confinement. By applying changes to the periodicity of the structure, it becomes possible to create a narrow range of sound waves that are allowed to pass through the structure in the range of the band gap. In fact, with this method, the sound wave is confined and directed in a narrow range of the band gap.[17] Achieving the phononic band gap and defect mode is the fundamental process in designing PhC devices. So far, many phononic structures have been presented in various fields[18,19] and designed structures with sensing performance will now be briefly discussed.

In 2019, Mehaney designed a PhC sensor for neutron detection. This structure is made of epoxy and concrete, which are repeated alternately in one dimension. When the structure is exposed to a neutron beam, due to the heat generated by the neutron beam, the Young's modulus of the materials that make up the structure changes and shows its effect in the width of the phononic band gap of structure.[20] Gharibi *et al.* proposed 2D PhC sensors with a steel background and water holes to sense the concentration of propanol in water. This structure includes a Mach–Zehnder defect with unequal pathways as the frequency resonator. Due to the asymmetry of the paths, the phase difference created in the passing sound wave is effective in removing excessive frequencies in the output, and this has an important effect on increasing the efficiency of the structure.[21] In other work, Gharibi and Mehaney introduced a 2D structure with water rods in a mercury background to detect the concentration of $H_2O_2$ in water. This sensor had a

[†]Corresponding author. E-mail: bahrami@sut.ac.ir

© 2024 Chinese Physical Society and IOP Publishing Ltd 

cavity defect as a frequency resonator with the target material embedded there. The performance parameters of this structure have a high sensitivity and quality factor for sensing.[7] Also, Khaligh *et al.* introduced a structure with hollow cylinders in the steel host and a cavity region to detect the acetic acid concentration in a vinegar mixture. The performance parameters of this structure show acceptable values. A quality factor of up to 40926 was obtained in the extremely fine mesh case.[22] In addition to sensor applications, these types of structures have also been used for temperature detection.[23] In addition to 2D structures, 3D structures have been investigated in a limited way; however, due to the complexity of building these structures, they have not been used much.[15] Considering all discussions, our aim is to conduct further research with more detail.

In this paper, a new method based on 2D PhCs with high sensitivity has been proposed to detect the percentage of $D_2O$ in an $H_2O$–$D_2O$ mixture. Results and transmission spectra of the incident acoustic wave were calculated by the finite element numerical method (FEM).

## 2. Design procedure

As a first step, a 2D solid–solid PhC structure is assembled as a square array of tungsten rods and an aluminum host. The value of the filling fraction of the structure is designed as $\pi r^2/a^2 = 0.5$, where $r = 4$ mm is radius of the scatterers and $a = 10$ mm is the lattice constant. Since the elastic properties of the materials used in the structure are very relevant to its behavior,[24] the properties of the materials used in this structure are also mentioned. Table 1 shows the physical parameters of the utilized materials.

**Table 1.** Elastic parameters of the materials utilized in the unit cell.

| Material | Mass density (kg/m$^3$) | Poisson's ratio | Young's modulus (GPa) |
|---|---|---|---|
| Aluminum | 2700 | 0.35 | 70 |
| Tungsten | 19350 | 0.28 | 411 |

In order to obtain the band diagram of the periodic structure, eigenfrequencies in the irreducible Brillouin zone (IBZ) were calculated by the Bloch–Floquet theory. In this way, periodic conditions on unit cell lateral boundaries must be applied and the wave vector ($k_x$, $k_y$) should be swept on both $\Gamma X$ and $\Gamma M$ directions of the IBZ. Figure 1 depicts the perfect structure of a unit cell including a tungsten rod in the aluminum host along with the corresponding band diagram.

According to Fig. 1(b), the band gap of this structure is wide at about 70 kHz. The wide range of forbidden gaps helps us to realize more targeted concentration sensing.

In order to guide the input signals to interact with the target material and receive the interacting signals at the output, a guiding channel must be created. Insofar as any changes in the periodicity of the structure lead to excessive modes in the phononic band gap, supercell analysis is necessary to detect the new modes. Figure 2 shows a supercell of the proposed guiding branch along with the results of supercell analysis.

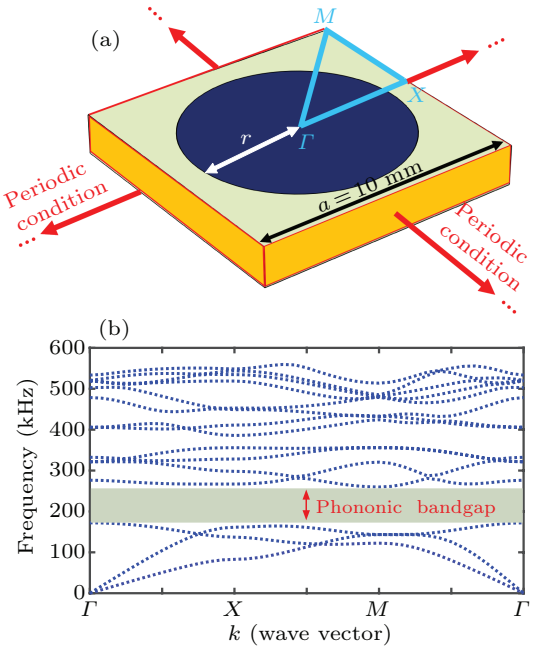



**Fig. 1.** (a) Schematic of the unit cell with the corresponding IBZ. (b) Calculated band diagram corresponding to the designed 2D PhC in the perfect case.

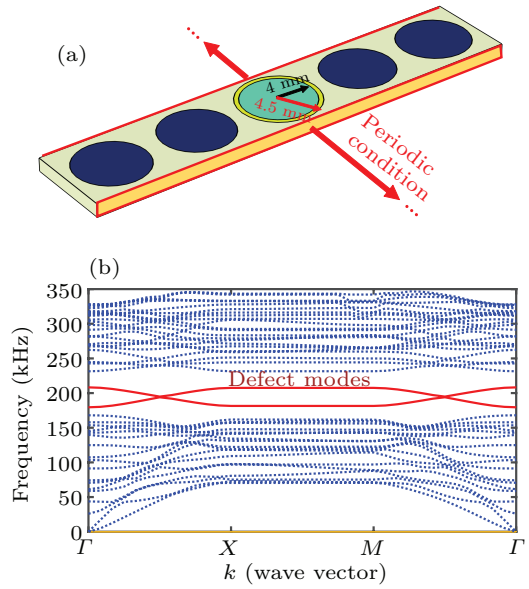



**Fig. 2.** (a) Overall view of a supercell of the waveguide. (b) Corresponding band diagram with two excessive defect modes (solid lines) in the forbidden region.

Figure 3(a) shows that the defect consists of a steel cylinder surrounded by a water shell. The radii of the steel and water cylinders are equal to 4 mm and 4.5 mm, respectively. Table 2 shows physical details of the defect materials.

Because the target sample is an $H_2O$–$D_2O$ mixture, a region should be considered for target testing and analysis. So, a cavity including an empty region with different concentrations of $D_2O$ mixtures for testing is embedded in the perfect

structure. Different concentrations of a mixture have different acoustic properties. The acoustic properties of $H_2O$ and $D_2O$ have been previously investigated at 20 °C and 1 atm conditions.[25,26] At $T = 20$ °C, the speed of sound and mass density of $D_2O$ are equal to 1383 m·s$^{-1}$ and 1054 kg·m$^{-3}$, respectively. As the amount of $D_2O$ in the mixture increases, the sound speed and density linearly decrease and increase, respectively, so we can estimate the acoustic parameters of the mixture with different concentrations of $D_2O$. Three-dimensional schematics of the optimized PhC structure are shown in Fig. 3.

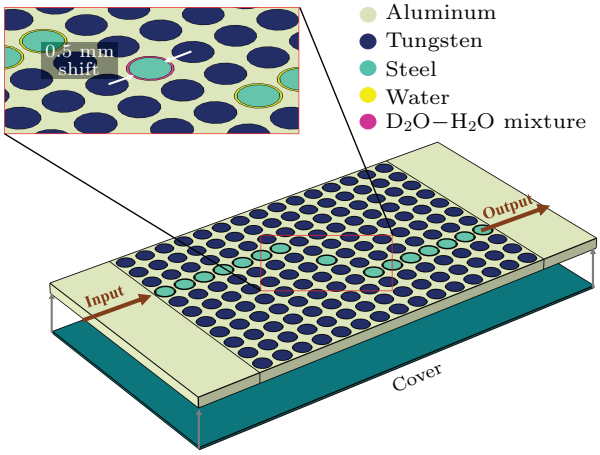



**Fig. 3.** Schematics of the complete proposed structure.

**Table 2.** Physical parameters of constituent materials in the defect.

| Material | Mass density (kg/m$^3$) | Speed of sound | Young's modulus (GPa) | Poisson's ratio |
|---|---|---|---|---|
| Stainless steel | 7780 | – | 210 | 0.28 |
| Water | 993 | 1483 | – | – |

In order to detect the target materials in the structure, a cavity is embedded inside it. The optimized dimensions of the cavity cylinders are the same as those of the waveguide cylinders. As can be seen in Fig. 5, to reach the optimum acoustic wave resonance in the cavity, the lateral rods in the cavity are been shifted inwards by 0.5 mm. The transmission spectrum of the complete structure with pure water inserted in the cavity (sensing region) is illustrated in Fig. 4.

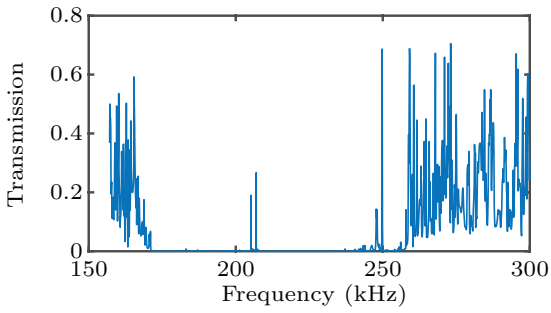



**Fig. 4.** Transmission spectrum of the complete structure with pure water in the cavity region.

According to the results, two resonance peaks are obtained in the band gap region. The resonance mode with a higher frequency is more suitable for sensing applications due to its larger amplitude. In the next section of this paper, transmission spectra of the structure for two concentration ranges (0%–10% and 90%–100%) of $D_2O$ in the $H_2O$–$D_2O$ mixture are obtained and analyzed.

## 3. Sensing

For sensing applications, different concentrations of the sample are added to the cavity region. The transmission spectra of the structure are illustrated in Fig. 5 for $D_2O$ concentrations in the mixture of 0%–10%, and Fig. 6 shows the shift of resonance peaks for concentrations of $D_2O$ in the mixture of between 90% and 100%.

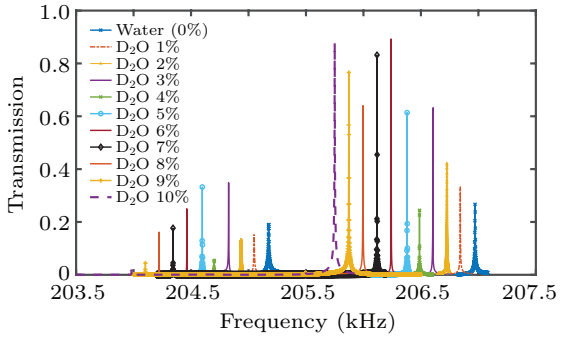



**Fig. 5.** Transmission spectra for diverse concentrations of $D_2O$ in an $H_2O$–$D_2O$ mixture (0%–10%).

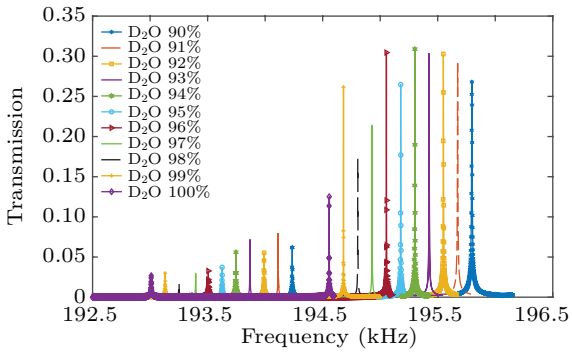



**Fig. 6.** Transmission spectra for diverse concentrations of $D_2O$ in an $H_2O$–$D_2O$ mixture (90%–100%).

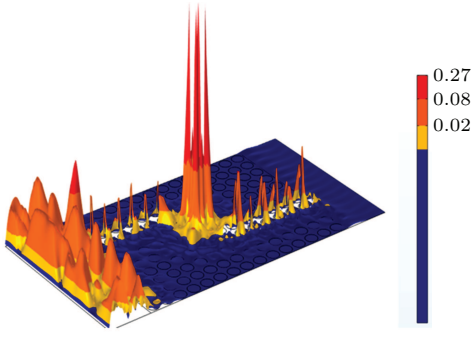



**Fig. 7.** Distribution field of applied wave with a frequency of 194.556 kHz through the final structure.

As mentioned before, for each concentration there are two resonance modes, but the resonance mode with a higher amplitude can be more practical and is chosen for sensing purposes. Extreme sharpness and sufficient frequency limitation from peak to peak enable the sensor to detect the target with minor concentration changes. Figure 7 shows field distributions of acoustic waves in the proposed sensor structure for an example frequency of 194.556 kHz.

In the next section the performance parameters of the structure according to the obtained results given in Tables 3 and 4 are calculated.

## 4. Sensor performance

Many factors can be used to evaluate sensor performance. In this section, we determine some important ones for analyzing the performance and capability of this sensor. The sensitivity index is calculated by[5]

$$S = \frac{\nabla f}{\nabla x}, \tag{1}$$

where the frequency limitation between each concentration of $D_2O$ compared with zero is defined as $\nabla f$, and $\nabla x$ corresponds to differences in concentration. The peak frequency of pure water is considered as zero.

Quality factor ($Q$) is another important index defined by the following equation:[5]

$$Q = \frac{f_r}{f_{1/2}}, \tag{2}$$

where the full width at half maximum (FWHM) of the resonant mode is $f_{1/2}$.

The equations below represent other important indices for sensor performance, the signal-to-noise ratio (SNR) and the figure of merit (FOM):[5]

$$\text{FOM} = \frac{S}{\nabla f_{1/2}}, \tag{3}$$

$$\text{SNR} = \frac{\nabla f}{\nabla f_{1/2}}. \tag{4}$$

The resolution index ($R$) is determined by the following equation:[5]

$$R = \frac{f_r}{Q}. \tag{5}$$

The calculated performance indices of the proposed $D_2O$ sensor are shown in Tables 3 and 4 for two concentration ranges corresponding to the transmission spectra depicted in Figs. 5 and 6. The parameters demonstrate very acceptable performance of the proposed sensor.

**Table 3.** The performance parameters of the $D_2O$ PhC sensor (0%–10% concentration range).

| $D_2O$ concentration (%) | Resonance frequency (kHz) | Sensitivity (Hz) | FWHM (Hz) | Quality factor | FOM | SNR | $R$ (Hz) |
|---|---|---|---|---|---|---|---|
| 0 ($H_2O$) | 206.971 | 0 | 6 | 34495.16 | – | – | 6 |
| 1 | 206.8426 | 12840 | 3.6 | 57456.27 | 3566.6 | 35.66 | 3.6 |
| 2 | 206.72605 | 12247.5 | 2 | 103363 | 6123.75 | 122.475 | 2 |
| 3 | 206.6062 | 12160 | 0.14 | 1475758.5 | 86857.14 | 2605.71 | 0.14 |
| 4 | 206.488 | 13075 | 2.8 | 73745.71 | 4669.64 | 172.5 | 2.8 |
| 5 | 206.380 | 11820 | 1.4 | 147414.2 | 8442.85 | 422.14 | 1.4 |
| 6 | 206.241 | 12166.66 | 1.46 | 141260.9 | 8333.3 | 500 | 1.46 |
| 7 | 206.118 | 12185.71 | 1.8 | 114510 | 6769.8 | 473.88 | 1.8 |
| 8 | 205.996 | 12187 | 2.8 | 73570 | 4352.5 | 348.21 | 2.8 |
| 9 | 205.873 | 12200 | 3.8 | 54177.1 | 3210.5 | 288.94 | 3.8 |
| 10 | 205.750 | 12210 | 4.5 | 45722.2 | 2713.3 | 271.33 | 4.5 |

**Table 4.** The performance parameters of the $D_2O$ PhC sensor (90%–100% concentration range).

| $D_2O$ concentration (%) | Resonance frequency (kHz) | Sensitivity (Hz) | FWHM (Hz) | Quality factor | FOM | SNR | $R$ (Hz) |
|---|---|---|---|---|---|---|---|
| 90 | 195.797 | 12415.5 | 7.4 | 26459 | 1677.7 | 1510 | 7.4 |
| 91 | 195673 | 12415.5 | 5.2 | 37629 | 2387.5 | 2172.6 | 5.2 |
| 92 | 195549 | 12415.2 | 3.9 | 50140.7 | 3183.3 | 2928.7 | 3.9 |
| 93 | 195425 | 12415.05 | 3 | 65141.6 | 4138.35 | 3848.6 | 3 |
| 94 | 195301 | 12414.8 | 2.35 | 83106.8 | 5282.8 | 4965.9 | 2.35 |
| 95 | 195178 | 12413.6 | 2.33 | 83767.3 | 5327.7 | 5061.3 | 2.33 |
| 96 | 195054 | 12413.5 | 1.6 | 121908.75 | 7758.43 | 7448.1 | 1.6 |
| 97 | 194930 | 12413.4 | 1.2 | 162441.6 | 10344.5 | 10034.1 | 1.2 |
| 98 | 194805 | 12414.2 | 2.33 | 83607.2 | 5327.9 | 5221.4 | 2.33 |
| 99 | 194681 | 12414.1 | 1.4 | 139057.8 | 8867.2 | 8778.5 | 1.4 |
| 100 ($D_2O$) | 194556 | 12415 | 2.6 | 74829.2 | 4775 | 4775 | 2.6 |

The sensitivity limitation is between 11820 and 13075 and the $Q$ factor reached a maximum value of 1475758 (minimum 26459). These parameters prove that the presented sensor has the best performance compared with the other phononic and PhC sensors proposed in the literature.[27,28]

## 5. Fabrication tolerance

Considering that errors that may occur during the construction process have an impact on the results obtained, we investigated the effect of these errors on the final results. Manufacturing errors may occur in any part of the structure, such as the lattice constant, the radius of the structural rods or the waveguide, etc. Here we only investigated the effect of changes in the radius of the rods in the waveguide part and the main part of the structure where the target material is placed. The results obtained for a 100% concentration of $D_2O$ with errors of $-0.2 < \Delta r < +0.2$ mm in the radii of the waveguide and cavity area containing $H_2O$ and $D_2O$ are shown in Figs. 8 and 9.

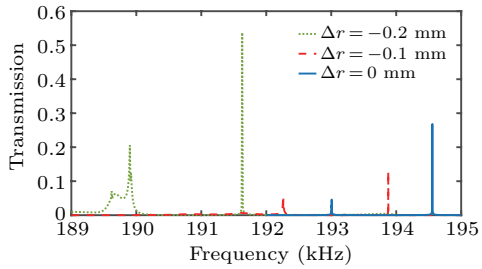



**Fig. 8.** The effect of changes in the radius of the waveguide and cavity on resonance peaks ($-0.2$ mm $< \Delta r < 0$).

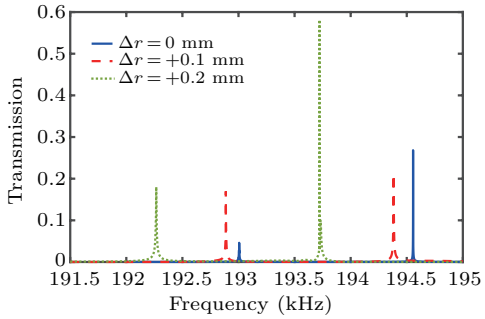



**Fig. 9.** The effect of changes in the radius of the waveguide and cavity on resonance peaks ($0 < \Delta r < +0.2$ mm).

As seen in Figs. 8 and 9, changes in the radius of the rods cause a shift in the resonance frequency. But the noteworthy point is that the changes in the radius have in each case reduced the resonant frequency, with the difference that reducing the radius from the optimal state causes more changes than increasing the radius from the optimal state.

## 6. Structural losses

Considering that the inherent characteristics of the materials used in the structure can cause losses in the applied sound wave, we investigated the effect of losses on the final result. The isotropic loss factor ($\eta_s$) of the metals used in the structure is considered as $0.5 \times 10^{-4}$. The dynamic viscosity ($\mu$) of $H_2O$ and $D_2O$ are taken as 1 mPa·s and 1.2 mPa·s, respectively, and their bulk viscosity ($\mu_b$) is taken as 2.4 mPa·s. The losses of the structure are calculated in percentage concentrations of 10% and 90% $D_2O$ and are compared with the values without losses in Figs. 10 and 11, respectively.

The results obtained from Figs. 10 and 11 show that the loss has no effect on the shift of the resonance peak and causes a reduction of the resonance peak amplitude compared with the state without losses. The change of resonance peak amplitude affects the sensor performance parameters that were introduced in Section 4. Therefore, the performance parameters of the sensor considering the losses in the structure were calculated and are shown in Table 5.

As can be seen in Table 5, the reduction of the amplitude of resonance peaks causes an unfavorable increase in the FWHM, and the increase of this key factor affects other performance evaluation parameters and reduces the quality of the structure.

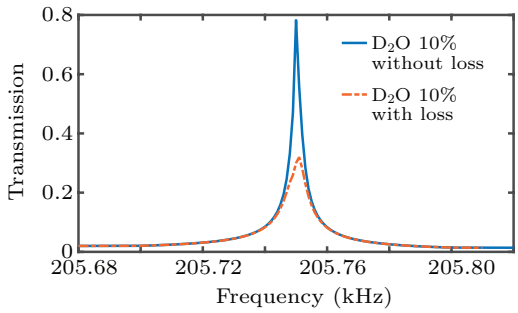



**Fig. 10.** Comparison of resonance peak changes in the state without losses compared with the state with losses for a percentage concentration of 10% $D_2O$ and resonance frequency of 205.750 kHz.

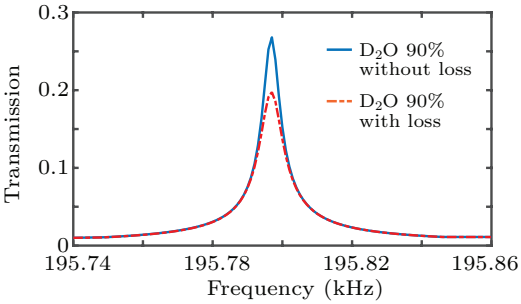



**Fig. 11.** Comparison of resonance peak changes in the state without losses compared with the state with losses for percentage concentration of 90% $D_2O$ and resonance frequency of 195.797 kHz

**Table 1.** Sensor performance parameters considering structural losses.

| $D_2O$ concentration (%) | Resonance frequency (kHz) | Sensitivity (Hz) | FWHM (Hz) | Quality factor | FOM | SNR | $R$ (Hz) |
|---|---|---|---|---|---|---|---|
| 10 | 205.750 | 12210 | 8 | 25718.7 | 1526 | 152.6 | 8 |
| 90 | 195.797 | 12415.5 | 9 | 21755 | 1356 | 1241 | 9 |

## 7. Conclusions

We have presented a phononic crystal structure for the purpose of detecting $D_2O$ concentration in the sensing field. In order to analyze the structure in the frequency domain, the finite element method was used. The resonance frequency of the cavity can be changed by modifying the $D_2O$ concentration. The frequency gap between each two neighboring peaks is about 120 Hz for each 1% change in concentration. The figure of merit results showed high-quality performance of the structure. Low cost and a simple manufacturing process are two reasons for using this sensing method rather than the other mentioned methods.

## References


[1] Herrig S, Thol M, Harvey A H and Lemmon E W 2018 *J. Phys. Chem. Ref. Data* **1** 47
[2] Lago S, Albo P G and Cavuoto G 2020 *Fluid Ph. Equilibria.* **15** 112401
[3] Kim J, Seo S and Kim T Y 2023 *Anal. Chim. Acta* **15** 1
[4] Rae H K 1978 *Jan. Am. Chem. Soc* (Washington DC)
[5] Dunning S G, Nuñez A J, Moore M D, Steiner A, Lynch V M, Sessler J L, Holliday B J and Humphrey S M 2017 *Chem* **2** 579
[6] Mir I A, Rawat K and Bohidar H B 2016 *Cryst. Res. Technol.* **51** 561
[7] Gharibi H and Mehaney A 2021 *Physica E* **126** 114429
[8] Gharibi H and Bahrami A 2020 *J. Mol. Liq.* **305** 112841
[9] Lucklum R, Ke M and Zubtsov M 2012 *Sens. Actuators B Chem.* **171** 271
[10] Lucklum R 2014 *Procedia Eng.* 2014 Jan **87** 40
[11] Villa-Arango S, Betancur D, Torres R and Kyriacou P 2018 *Sensors* **18** 3618
[12] Alrowaili Z A, Fathy H M, Elsayed H A, Aouassa M, Mahmoud M H, El-Nasser K S, Taha T A and Mehaney A 2023 *Ultrasonics* **130** 106928
[13] Miao X B, Dong H W and Wang Y S 2023 *Eng. Optim.* **55** 125
[14] Rahimi M R and Bahrami A 2022 *ISAV2022 Amirkabir University of Technology* (Tehran Polytechnic), Iran pp. 1–6
[15] Lucklum F and Vellekoop M J 2016 *IEEE Sensors* pp. 1–3
[16] Gueddida A, Zhang V, Carpentier L, Bonhomme J, Bonello B, Pennec Y and Djafari-Rouhani 2023 *Sensors* **23** 2080
[17] Mukhin N, Kutia M, Aman A, Steinmann U and Lucklum R 2022 *Sensors* **22** 2816
[18] Motaei F and Bahrami A 2022 *Sci. Rep.* **12** 10522
[19] Motaei F and Bahrami 2020 *J. Mater. Sci.* **55** 8983
[20] Mehaney A 2019 *Ultrasonics* **93** 37
[21] Gharibi H, Khaligh A, Bahrami A and Ghavifekr H B 2019 *J. Mol. Liq.* **296** 111878
[22] Khaligh A, Bahrami A and Ghavifekr H B 2021 *J. Mol. Liq.* **343** 116972
[23] Zaremanesh M, Carpentier L, Gharibi H, Bahrami A, Mehaney A, Gueddida A, Lucklum R, Djafari-Rouhani B and Pennec Y 2021 *APL Mater.* 9
[24] Wu Y, Lai Y and Zhang Z Q 2011 *Phys. Rev. Lett.* **107** 105506
[25] Wilson W D 1961 *JASA* **1961** 314
[26] Schaaffs W 1967 *Molecular Acoustics* Springer-Verlag (Berlin, Germany)
[27] Bhardwaj V and Singh V K 2016 *Sens. Actuator A Phys.* **244** 30
[28] Mehaney A 2020 *MRX* **6** 125556